SCIENCE CHINA
Chemistry

• ARTICLES •

A Thermally Reversible Dynamic Bond as a Magnetic and Nonlinear Optical Switch

Xue-Li Cao,[1,2,3]† Jin Liu,[1,2,3]† Chuan-Qi Shen,[1,2] Shu-Qi Wu,[4]* Zi-Shuo Yao,[5] Qing Li,[1,2,3] Zhong-Min Cao,[1,2,3] Lu-Yao Liu,[1,2,3] Fu-Lin Lin,[1,2] Zi-Ang Nan,[1,2] Zhu Zhuo,[1,2] Wei Wang,[1,2] Osamu Sato,[4] and You-Gui Huang[1,2,3]*

[1] *State Key Laboratory of Structure Chemistry, Fujian Institute of Research on the Structure of Matter, Chinese Academy of Science, Fuzhou, Fujian, 350002, China*

[2] *Fujian Science & Technology Innovation Laboratory for Optoelectronic Information of China*

[3] *Xiamen Key Laboratory of Rare Earth Photoelectric Functional Materials, Xiamen Institute of Rare Earth Materials, Haixi Institutes, Chinese Academy of Sciences, Xiamen, Fujian, 361021, China*

[4] *Institute for Materials Chemistry and Engineering & IRCCS, Kyushu University, 744 Motooka, Nishi-ku, Fukuoka, Japan*

[5] *Key Laboratory of Cluster Science of Ministry of Education, School of Chemistry and Chemical Engineering, Beijing Institute of Technology, Beijing, China*

Received ***; accepted ***; published online ***

In general, flexible metal-organic frameworks (MOFs) change their structures via framework breathing in response to external stimuli (usually guest adsorption and desorption). Here, we show a dynamic coordination bond in a flexible MOF driving a thermo-induced diffuse phase transition occurring in a wide temperature range of 130–270 K (centered at ~200 K), which enables the switching of magnetism and second-harmonic generation (SHG) responses. In specific, a solvent-free Co^{II}-based flexible MOF $Co_2(TPY)_2(BPTC)$ (**1**), bearing biphenyl-3,3',5,5'-tetracarboxylic acid (H_4BPTC) and 2,2':6',2''-terpyridine (TPY) ligands, exhibits a reversible thermo-responsive coordination-mode switching between five- and six-fold. This dynamic bond results in the reversible transformation between a distorted polar framework and a regular nonpolar framework, and therefore leads to the subtle change of the magnetic property and substantial change of the nonlinear optical property of **1**.

Flexible, Metal-Organic Framework, Switch, Magnetism, Second-Harmonic Generation

Citation: Cao XL, Liu J, Shen CQ, Wu SQ, Yao ZS, Li Q, Cao ZM, Liu LY, Lin FL, Nan ZA, Zhuo Z, Wang W, Sato O, Huang YG, A Thermally Reversible Dynamic Bond as a Magnetic and Nonlinear Optical Switch. Sci China Chem, 2024,

1 Introduction

The variable coordination geometry of transition metal centers and the lability of coordination bonds allow flexible MOFs to exhibit reversible structural transitions under external stimuli.[1-8] These stimuli-induced transitions endow a wide range of functional properties such as "gate-opening adsorption",[9-13] metal–insulator transition,[14, 15] magnetic bistability,[16] and ferroelectricity.[17-20] Typically, structural transformations in porous flexible MOFs rely on the guest incorporation/removal, which might enable discriminatory gate-opening behaviors. However, reversible thermo-induced phase transitions leading to the switching of MOF's physical properties are far less common, let alone the thermo-induced phase transitions involving bond cleavage and formation.[21-24] This may be attributed to the fact that few dynamic metal–ligand bonds can be accessible for MOFs.[25]

It is well known that ligands bearing multiple carboxyl groups can be used to construct MOFs.[26-31] For the coordi-

*Corresponding authors (email: wu.shuqi.152@m.kyushu-u.ac.jp; yghuang@fjirsm.ac.cn)

nation of carboxyl groups, the thermo-responsive monodentate/bidentate switching behaviors have been observed in nonheme diiron proteins.[24] Therefore, we propose to harness the labile metal–carboxylate coordination to introduce dynamic bonds into MOFs. This could potentially realize the thermal switching of certain physical properties. Our previous efforts on thermo-responsive materials have identified a hydrogen-bonded framework (HOF) showing a temperature-induced phase transition governed by the dynamic hydrogen bonds between H_4BPTC and 4,4'-azopyridine (azpy).[32, 33] We envisage that the thermo-responsive dynamic coordination bonds may be accessed in flexible MOFs bearing the $BPTC^{4-}$ ligands, provided that the structural flexibility can tolerate the bond switching. If the proposed thermo-induced phase transition can be realized, switchable physical properties might be readily achievable providing potential for new memory devices.[34] For example, switchable magnetic moment can be realized when the phase transition is correlated to the change of the chemical environment of paramagnetic centers[35-38] as observed on the spin crossover compounds[39-47] and the compounds with switchable orbital angular momentum[23, 48]. Furthermore, symmetry breaking may be introduced into the phase transition of magnetic materials[42] and thus switching of multiple physical properties can be expected.

Herein, we report a solvent-free two-dimensional (2D) flexible MOF $Co_2(TPY)_2(BPTC)$ (**1**) comprising $[Co(TPY)]^{2+}$ and $BPTC^{4-}$. **1** undergoes a thermo-induced phase transition involving metal–carboxylate bond switching and framework-deformation. The transition temperatures are in a wide range of 130–270 K with the center at ~200 K. Upon cooling, the Co^{II} ions change the coordination number from five to six, and two of the carboxyl groups of the $BPTC^{4-}$ ligand change their coordination modes from monodentate to bidentate accordingly. Simultaneously, the formation of the sixth coordination bond changes the framework from a nonpolar structure to a distorted polar structure. Along with the phase transition, the magnetic and nonlinear optical properties of **1** also switch reversibly.

2 Results and Discussion

The solvothermal reaction of $CoCl_2$, TPY, and H_4BPTC in methanol affords pink crystals of **1·solvent**. Single-crystal X-ray crystallography at 328 K reveals a grid layer structure with one-dimensional (1D) regular "wine-rack" channels. **1·solvent** (the high-temperature (HT) phase) crystallizes in the centrosymmetric space group *Fddd* (Table S1), and the asymmetric unit comprises half of a $[Co(TPY)]^{2+}$ cation and one fourth of a $BPTC^{4-}$ ligand. The strong absorption at 1574 cm^{-1} in the infrared (IR) spectrum of **1·solvent** can be assigned to $\upsilon_{C=O}$ from the carboxyl groups in $BPTC^{4-}$ (Figure S1).[49] The Co^{II} ion is in five-fold coordination by three N atoms from the same TPY and two O atoms from two carboxyl groups of two different $BPTC^{4-}$ ligands (Figure S2a). The two carboxyl groups are located on both sides of the plane defined by the $[Co(TPY)]^{2+}$ cation, adopting the monodentate η^1-coordination mode with the same Co–O distance of 2.033 Å. The $BPTC^{4-}$ ligands act as tetra-topic linkers connecting the $[Co(TPY)]^{2+}$ ions into a 2D grid framework in the *ab* plane (Figures 1a and S2a). The grid layer structures slip-stack along the *c* axis (Figure 1b), forming a centrosymmetric structure with "wine-rack" channels along both [1 0 0] and [1 1 0] directions (Figure 1c).

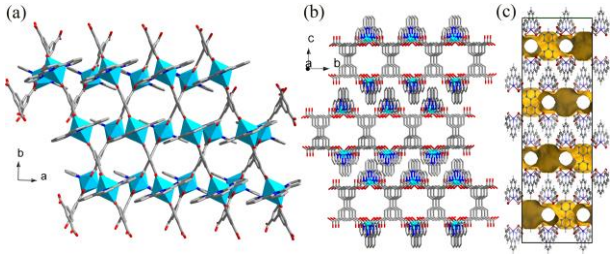

Figure 1 (a) The grid layer structure of **1·solvent**. (b) The slip-stacked layer structure of **1·solvent**. (c) The "wine-rack" channels in the crystal structure of **1·solvent**.

Thermogravimetric analysis (TGA) shows that the framework of **1** is stable up to about 400 °C, with the mass loss (~10.52 wt%) between 30 and 100 °C attributed to the removal of solvent molecules in the channels (Figure S3). The framework remains intact after desolvation, as confirmed by the powder X-ray diffraction (PXRD) measurements (Figure S4). The excellent thermos-stability of **1** promote us to evaluate its permanent porosity. The N_2 sorption isotherm measured at 77 K on **1** gives a Brunauer-Emmett-Teller (BET) surface area of 487 $m^2\ g^{-1}$, a pore volume of 0.225 $cm^3\ g^{-1}$, and a narrow pore size distribution with an average pore diameter of 9.02 Å (Figure S5). These values are consistent with the structural analysis. Furthermore, the CO_2 isotherms measured at 195, 273, and 298 K reveal an uptake of 80.74, 60.74, and 45.76 cm^3 (STP) g^{-1} at $P/P_0 = 1$, respectively (Figure S6a). The isosteric heat of adsorption (Q_{st}) at zero coverage is estimated to be 31.2 kJ mol^{-1} using the adsorption isotherms at 273 and 298 K (Figures S6b and S7). No obvious hysteresis can be observed for all of the isotherms, indicating that the framework is robust in response to the gas sorption.[50]

When the temperature decreases, a structural transition occurs. The single-crystal structure analysis at 200 K showed that **1·solvent** transfers to a low-temperature (LT) phase, which crystallizes in a non-centrosymmetric space group *Fdd2* (Table S1). This implies that a symmetry breaking process has occurred. The LT structure is best refined using the two-component inversion twin strategy giv-

ing a Flack parameter of ~0.5 implying the transition involving a transformation from a single crystal with single domain to a twinned single crystal with multi domains.[51] Compared with the HT phase, the asymmetric unit of the LT phase is doubled, containing a $[Co(TPY)]^{2+}$ ion and half of a $BPTC^{4-}$ ligand. In response to the decreasing temperature, the $BPTC^{4-}$ ligands tilt substantially. The benzene rings of the $BPTC^{4-}$ tilt from orthogonal to the plane defined by the $[Co(TPY)]^{2+}$ ions at HT, to an angle of 70.5° at LT (Figure 2b). Accordingly, three significant structural changes occur : (1) a new Co–O bond Co–O4 (with the Co–O4 and Co–O2 distances both 2.671 Å in the HT phase) change to (2.382 and 2.934 Å, respectively, in the LT phase) forms leading to the Co^{II} ions change from five-coordination to six-coordination (Figures 2a and S2a); (2) two carboxyl groups from the same $BPTC^{4-}$ ligand change to the asymmetric bidentate η^2-coordination mode (Figures 2a and S2b); (3) the "wine-rack" channels distort dramatically from the HT phase (Figure 2b), resulting in the change of the solvent accessible pore volume from 27.6% in the HT phase to 26.3% in the LT phase.

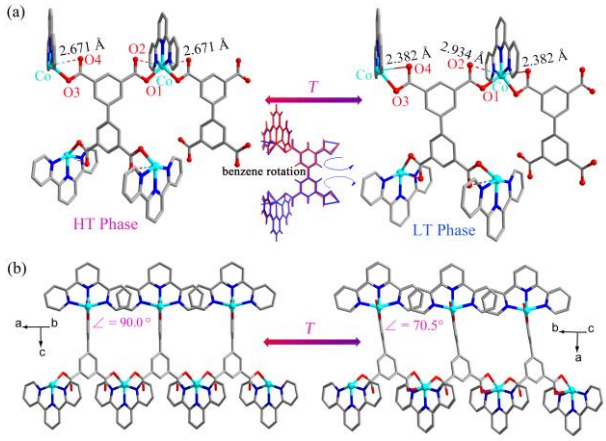

Figure 2 (a) The variation of the coordination of Co^{2+} ions and $BPTC^{4-}$ during the thermo-induced phase transition. (The atoms are labeled in accordance with those in the LT phase.) (b) The distortion of the 2D framework during the phase transition.

Since the components of the solvent molecules were failed to be determined by SCXRD on this strategy, another single crystal of **1·solvent** was picked out for structural determination at 200 K initially and then at 328 K. In this case, the solvent molecules can be clearly identified and the formula for **1·solvent** was determined to be $Co_2(TPY)_2(BPTC)(CH_3OH)_{0.5}(H_2O)_3$ which is consistent to the TGA result and further confirmed by elemental analysis.

Although relatively weaker than the conventional Co–O coordination bonds, the interaction of Co–O4 (2.382 Å) in the LT phase can be assigned to be a bond path.[22] The bond length of C23=O4 is significantly increased from 1.238 Å in the HT phase to 1.257 Å in the LT phase, which also indicates the switching from the monodentate η^1-coordination to the bidentate η^2-coordination of the corresponding carboxyl group (O3–C23–O4) (Figure S2b). Furthermore, the apparent bonding of Co–O4 is also indicated by the theoretical computation, which suggests notable attraction between these two atoms (Figure S8). To clarify which external stimuli (*e.g* temperature or guest) triggers the phase transition of **1·solvent**, structural determinations are also performed on a single-crystal of **1** (solvent free sample) at 270 K, 255 K, 305 K, and 260 K during the heating and cooling cycles of 350–200–350–200 K. The results confirm that **1** also undergoes the phase transition reversibly (Table S3), precluding the possibility of guest-dependent phase transition. The molecular movements during the phase transition induce the symmetry breaking from the HT phase with eight symmetry elements (E, $3C_2$, i, σ_v, σ_h, and σ_d) to the LT phase with four (E, C_2, σ_v, and σ_d), which is in good agreement with a ferroelectric-to-paraelectric transition with the Aizu notation *mmmFmm2*.[52]

The thermo-induced phase transition of **1** is further monitored using the differential scanning calorimetry (DSC) and heat capacity (C_p) measurements. DSC curves (at a rate of 5 K/min) reveal a reversible phase transition with very broad peaks (Figure 3a). The heating branch shows a broad Exo thermic peak (130–270 K) centered at ~203 K, and the corresponding Endo thermic peak on the cooling branch appears in the range of (134–274 K) with the peak center at ~199 K. The transition enthalpy (ΔH) and entropy (ΔS) estimated from the DSC measurement are $\Delta H \approx 7.74$ kJ mol^{-1} and $\Delta S \approx 38.1$ J K^{-1} mol^{-1}, respectively. The C_p–T plot shows a slight anomaly from 150 to 270 K (Figure S9), but the first-order derivative of the C_p–T plot shows a broad peak (130–272 K) centered at ~202 K (Figure 3b) indicating a second order phase transition.[53]

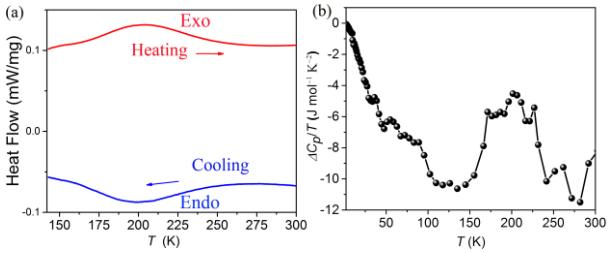

Figure 3 (a) DSC curves of **1** showing the reversible phase transition. (b) The $\Delta C_p/T$–T plot of **1** from 2 to 300 K at a rate of 5 K/min.

Because the phase transition involves the variation of the coordination environment of paramagnetic Co^{II}, the temperature-variable magnetic susceptibilities were measured on **1** (solvent free sample) in a cycle of 400–2–400 K under 1000 Oe to investigate the corresponding change of magnetism (Figures 4, S10). During the cooling course, the $\chi_m T$ value per Co^{II} slightly decreases from 2.58 cm^3 K mol^{-1} at 400 K to 2.50 cm^3 K mol^{-1} at ~200 K, and then slightly increases before quickly decreasing at ~100 K. During the heating

course, the $\chi_m T$ value per Co^{II} increases to a maximum of 2.53 cm^3 K mol^{-1} at 126 K, and then decreases to a minimum at ~200 K before gradually increasing. Remarkably, an obvious small hysteresis can be observed, probably due to the small thermal hysteresis and/or irreversible pathway of the phase transition. The minimum observed at ~200 K during both the courses was caused by the phase transition, consistent to transition temperatures suggested by DSC and heat capacity measurements. Even the minimum $\chi_m T$ value at ~200 K is between the values for high-spin Co^{II} with a fully quenched (1.88 cm^3 mol^{-1} K) and unquenched (5.49 cm^3 mol^{-1} K) angular momentum, indicating a significant contribution of the angular momentum for both phases.[23] Fitting the magnetic susceptibilities from the heating course (200–400 K) with the Curie–Weiss law gives a Curie constant of C = 2.70 cm^3 K mol^{-1} and a Weiss constant θ = –17.9 K for the HT phase) (Figure S11). The corresponding results for the LT phase (45–115 K) are C = 2.70 cm^3 K mol^{-1} and θ = –7.36 K. The same Curie constant for the HT and LT phases gives the same g value (g_{HT} = g_{LT} = 2.40), and the different magnetic properties primarily originate from the significantly different Weiss temperatures (θ).

For Co^{II} without apparent magnetic coupling, θ is closely related to magnetic anisotropy induced by spin–orbital coupling which can be reflected by phenomenological magnetic parameters: D, $|E|$, and giso, where D and E are the axial and rhombic anisotropic parameters respectively; and giso is the isotropic g factor. To interpret our experimental observations and provide insights into the observed magnetism switching, *ab initio* calculations using the CASSCF/NEVPT2 (Complete-Active-Space Self-Consistent-Field/2nd-order N-electron valence state perturbation theory) protocol were performed. The $\chi_m T$–T plots obtained by the quasi-degenerate perturbation theory agree with the experimental observation (Figures 4, S10). Projecting the calculated low-lying doublets onto the spin Hamiltonian with S = 3/2 yields the following phenomenological magnetic parameters: D = 42.1 cm^{-1}, $|E|$ = 8.36 cm^{-1}, and giso = 2.25 (g_x = 1.99, g_y = 2.28, g_z = 2.47) for the HT phase; and D = 46.5 cm^{-1}, $|E|$ = 10.9 cm^{-1}, and giso = 2.27 (g_x = 1.98, g_y = 2.30, g_z = 2.54) for the LT phase, which are reasonable compared with the parameters from the experimental data. The different values of D and $|E|$ indicate the observed slight change in magnetic moments is ascribed to the switching of magnetic anisotropy of Co^{II} between these two phases. The orbital contributions to g-factors of the ground doublet change obviously; the ratio of isotropic orbital contribution and spin contribution (g_L/g_S) increase from 0.048 for the HT phase to 0.091 for the LT phase (Table S5).

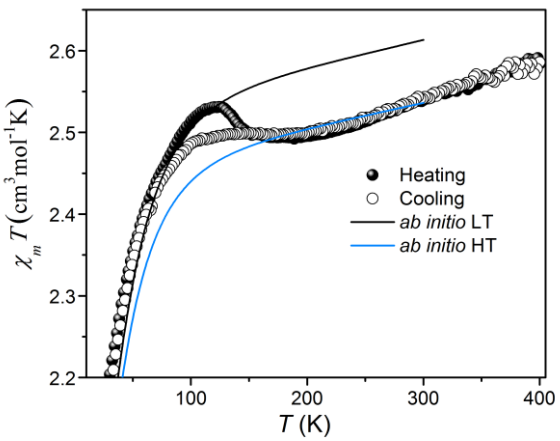

Figure 4 The $\chi_m T$–T plots of **1** in the range of 20–400 K during the cooling and heating cycle of 400–2–400 K at a rate of 4 K/min.

The orbital diagrams for the LT and HT phases were further calculated using *ab initio* ligand-field theory (AILFT) (Figure S12). Due to the different coordination geometries, the Co^{II} ions show different d-orbital splitting in the LT and HT phases. In the HT phase, the splitting of the three low-lying d-orbitals occurs at 372 and 3161 cm^{-1}. This can be understood from the energy differences within the quasi-degenerate e orbital and b_1 orbital in a pseudo-square pyramidal coordination environment. In the LT phase, structural distortions cause additional changes in these splitting energies, which contribute differently to the magnetic anisotropy of Co^{II} and result in a slight change in the magnetic properties.

Since the phase transition results in the change from a centrosymmetric structure to a non-centrosymmetric one, spontaneous polarization will appear in the LT phase.[54-56] We calculated the dipole moment of the subunit {Co_2(TPY)$_2$(BPTC)} and obtained an approximate value of 3.54 Debye for the LT phase (Figure S13). The quenching of the theoretical dipole moment from the LT to HT phase suggests that the dynamic bond Co–O4 may act as a SHG switch. Therefore, temperature variable SHG measurements are performed on **1** from 90 to 320 K. As shown in Figure 5, the SHG intensity gradually decreased upon heating reaching about zero at 250 K, confirming the transition to a centrosymmetric structure (HT phase) from the non-centrosymmetric LT phase. In addition, the disappearance of the bright green spot at high temperatures further confirms the emergence of inversion symmetry at the HT phase (Figure 5b, inset).[57] Furthermore, the SHG intensity switching can be manipulated repeatably as shown in Figure S14.

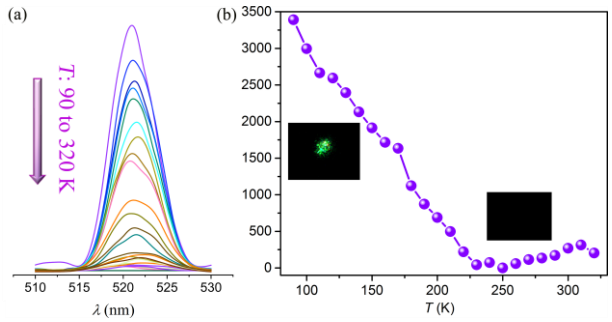

Figure 5 (a) The SHG signals of **1** at various temperature. (b) Variation of the SHG intensity of **1** upon heating.

3 Conclusions

In conclusion, we demonstrate the temperature-induced framework deformation of a flexible MOF, triggered by a dynamic metal–carboxylate bond. The subtle structural change alters the corresponding physical properties including the magnetic and non-linear optical properties. Understanding the switching mechanism of this unique phase transition process provides important insights into the design of framework materials that are capable of reversible switching between different stable phases upon stimulation.

Acknowledgments This work was Supported by the National Natural Science Foundation of China (92261109 and 22371280), Natural Science Foundation of Fujian Province (2023J01219), Project Funded by China Postdoctoral Science Foundation (No. 2023M733496), the Recruitment Program of Global Youth Experts, XIREM autonomously deployment project (No.2023GG02), FJIRSM autonomously deployment project (CXZX-2022-GH02), and Youth Innovation Promotion Association CAS (2021302).

Conflict of interest The authors declare no conflict of interest.

Supporting information The supporting information is available online at http://chem.scichina.com and http://link.springer.com/journal/11426. The supporting materials are published as submitted, without typesetting or editing. The responsibility for scientific accuracy and content remains entirely with the authors.

1 Grobler I, Smith VJ, Bhatt PM, Herbert SA, Barbour LJ. *J Am Chem Soc*, 2013, 135: 6411–6414
2 Li W, Probert MR, Kosa M, Bennett TD, Thirumurugan A, Burwood RP, Parinello M, Howard JA, Cheetham AK. *J Am Chem Soc*, 2012, 134: 11940–11943
3 Sen S, Hosono N, Zheng JJ, Kusaka S, Matsuda R, Sakaki S, Kitagawa S. *J Am Chem Soc*, 2017, 139: 18313–18321
4 Zhang JP, Liao PQ, Zhou HL, Lin RB, Chen XM. *Chem Soc Rev*, 2014, 43: 5789–5814
5 Schneemann A, Bon V, Schwedler I, Senkovska I, Kaskel S, Fischer RA. *Chem Soc Rev*, 2014, 43: 6062–6096
6 Bennett TD, Cheetham AK, Fuchs AH, Coudert FX. *Nat Chem*, 2017, 9: 11–16
7 Choi HS, Suh MP. *Angew Chem Int Ed*, 2009, 48: 6865–6869
8 Deng H, Olson MA, Stoddart JF, Yaghi OM. *Nat Chem*, 2010, 2: 439–443
9 Zhang PD, Wu XQ, He T, Xie LH, Chen Q, Li JR. *Chem Commun*, 2020, 56: 5520–5523
10 Zheng JJ, Kusaka S, Matsuda R, Kitagawa S, Sakaki S. *J Am Chem. Soc*, 2018, 140:13958–13969
11 Banerjee D, Wang H, Plonka AM, Emge TJ, Parise JB, Li J. *Chem Eur J*, 2016, 22: 11816–11825
12 Chen DL, Wang N, Wang FF, Xie J, Zhong Y, Zhu W, Johnson JK, Krishna R. *J Phys Chem C*, 2014, 118: 17831–17837
13 Seo J, Bonneau C, Matsuda R, Takata M, Kitagawa S. *J Am Chem Soc*, 2011, 133: 9005–9013
14 O'Hara A, Demkov AA. *Phys Rev B*, 2015, 91: 094305
15 Ueda A, Yamada S, Isono T, Kamo H, Nakao A, Kumai R, Nakao H, Murakami Y, Yamamoto K, Nishio Y, Mori H. *J Am Chem Soc*, 2014, 136: 12184–2192
16 Zhao XH, Huang XC, Zhang SL, Shao D, Wei HY, Wang XY. *J Am Chem Soc*, 2013, 135: 16006–16009
17 Wu YQ, Zhang JY, He X, Wang ZX, Cai HL, Li MX. *Cryst Growth Des*, 2021, 21: 6245–6253
18 Lee JY, Ling S, Argent SP, Senn MS, Cañadillas-Delgado L, Cliffe MJ. *Chem Sci*, 2021, 12: 3516–3525
19 Liu C, Zhai K, Yu Z, Nie A, Liu Z, Sun Y. *J Phys Chem C*, 2020, 124: 16111–16115
20 Xin L, Zhang Z, Carpenter MA, Zhang M, Jin F, Zhang Q, Wang X, Tang W, Lou X. *Adv Funct Mater*, 2018, 28: 1806013
21 Xu WJ, Li PF, Tang YY, Zhang WX, Xiong RG, Chen XM. *J Am Chem Soc*, 2017, 139: 6369–6375
22 Pan F, Wang R, Englert U. *Inorg Chem*, 2012, 51: 769–771
23 Su SQ, Wu SQ, Baker ML, Bencok P, Azuma N, Miyazaki Y, Nakano M, Kang S, Shiota Y, Yoshizawa K, Kanegawa S, Sato O. *J Am Chem Soc*, 2020, 142: 11434–11441
24 Burger B, Dechert S, Grosse C, Demeshko S, Meyer F. *Chem Comm*, 2011, 47: 10428–10430
25 Obeso JL, Huxley MT, Leyva C, Flores JG, Martín-Guaregua N, Viniegra M, Aguilar-Pliego J, de los Reyes JA, Ibarra IA, Peralta RA. *Coord Chem Rev*, 2023, 496: 215403
26 Andreeva AB, Le KN, Chen L, Kellman ME, Hendon CH, Brozek CK. *J Am Chem Soc*, 2020, 142: 19291–19299
27 Huang YG, Wu SQ, Deng WH, Xu G, Hu FL, Hill JP, Wei W, Su SQ, Shrestha LK, Sato O, Wu MY, Hong MC, Ariga K. *Adv Mater*, 2017, 29: 1703301
28 Huang YG, Yuan DQ, Pan L, Jiang FL, Wu MY, Zhang XD, Wei, Gao Q, Lee JY, Li J, Hong MC. *Inorg Chem*, 2007, 46: 9609–9615
29 Eddaoudi M, Kim J, Rosi N, Vodak D, Wachter J, O'Keeffe M, Yaghi OM. *Science*, 2002, 295: 469–472
30 Li H, Eddaoudi M, Groy TL, Yaghi OJ. *J Am Chem Soc*, 1998, 120: 8571–8572
31 Yang L, Cai P, Zhang L, Xu X, Yakovenko AA, Wang Q, Pang J, Yuan S, Zou X, Huang N, Huang Z, Zhou HC. *J Am Chem Soc*, 2021, 143: 12129–12137
32 Huang YG, Shiota Y, Su SQ, Wu SQ, Yao ZS, Li GL, Kanegawa S, Kang S, Kamachi T, Yoshizawa K, Ariga K, Sato O. *Angew Chem Int Ed*, 2016, 55: 14628–14632
33 Huang YG, Shiota Y, Wu MY, Su SQ, Yao ZS, Kang S, Kanegawa S, Li GL, Wu SQ, Kamachi T, Yoshizawa K, Ariga K, Hong MC, Sato O. *Nat Commun*, 2016, 7: 11564
34 Sakata Y, Furukawa S, Kondo M, Hirai K, Horike N, Takashima Y, Uehara H, Louvain N, Meilikhov M, Tsuruoka T, Isoda S, Kosaka W, Sakata O, Kitagawa S. *Science*, 2013, 339: 193–196
35 Fukunaga H, Tonouchi M, Taniguchi K, Kosaka W, Kimura S, Miyasaka H. *Chem Eur J*, 2018, 24: 4294–4304
36 Talin AA, Centrone A, Ford AC, Foster ME, Stavila V, Haney P, Kinney RA, Szalai V, El Gabaly F, Yoon HP, Léonard F, Allendorf MD. *Science*, 2014, 343: 66–69
37 Das D, Ghosh A, Pariya C, Chaudhuri NR. *J Chem Res*, 2016, 656: 439–442
38 Vologzhanina AV, Belov AS, Novikov VV, Dolganov AV, Romanenko GV, Ovcharenko VI, Korlyukov AA, Buzin MI, Voloshin YZ. *Inorg Chem*, 2015, 54: 5827-5838
39 Seredyuk M, Znovjyak K, Valverde-Muñoz FJ, Muñoz MC, Fritsky IO, Real JA. *Dalton Trans*, 2024, 53: 8041-8049
40 Zenno H, Sekine Y, Zhang Z, Hayami S. *Dalton Trans*, 2024, 53: 5861-5870
41 Janetzki JT, Chegerev MG, Gransbury GK, Gable RW, Clegg JK, Mulder RJ, Jameson GN, Starikova AA, Boskovic C. *Inorg Chem*,

2023, 62: 15719-15735
42 Zhang X, Xu W-H, Zheng W, Su S-Q, Huang Y-B, Shui Q, Ji T, Uematsu M, Chen Q, Tokunaga M, Gao MG, Okazawa A, Kanegawa S, Wu SQ, Sato O. *J Am Chem Soc*, 2023, 145: 15647–15651
43 Tailleur E, Marchivie M, Negrier P, Denux D, Massip S, Mondieig D, Chastanet G, Guionneau P. *CrystEngComm* 2019, 21: 6246-6251
44 Phonsri W, Lewis BA, Jameson GN, Murray KS. *Chem Commun*, 2019, 55: 14031-14034
45 Gütlich P, Garcia Y, Goodwin HA. *Chem Soc Rev*, 2000, 29: 419-427
46 Batten SR, Bjernemose J, Jensen P, Leita BA, Murray KS, Moubaraki B, Smith JP, Toftlund H. *Dalton Trans*, 2004, 20: 3370-3375
47 Berdiell IC, Kulmaczewski R, Shahid N, Cespedes O, Halcrow MA. *Chem Commun*, 2021, 57: 6566-6569
48 Juhász G, Matsuda R, Kanegawa S, Inoue K, Sato O, Yoshizawa K. *J Am Chem Soc*, 2009, 131: 4560-4561
49 Zhuo Z, Huang Y-G, Walton KS, Sato O. *Front Chem*, 2020, 8: 506
50 Zhuo Z, Li GL, Shu CL, Wang W, Liu CP, Wu MY, Huang YG, Hong MC. *Sci China Chem*, 2021, 64: 22-28
51 Chen G, Peng YB, Zheng G, Qi ZX, Wang MZ, Yu HC, Dong CL, Liu CT. *Nat Mater*, 2016, 15: 876-881
52 Aizu K. *Phys Rev B*, 1970, 2: 754–772
53 Kuo CN, Chen WT, Tseng CW, Hsu CJ, Huang RY, Chou FC, Kuo YK, Lue CS. *Phys Rev B,* 2018, 97: 094101
54 Yao ZS, Yamamoto K, Cai HL, Takahashi K, Sato O. *J Am Chem Soc*, 2016, 138: 12005-12008
55 Sun Z, Chen T, Luo J, Hong M. *Angew Chem Int Ed*, 2012, 51: 3871-3876
56 Wang S, Liu X, Li L, Ji C, Sun Z, Wu Z, Hong M, Luo J. *J Am Chem Soc*, 2019, 141: 7693-7697
57 Yamamoto K, Kowalska AA, Yakushi K. *Appl Phys Lett*, 2010, 96

Table of Contents graphic

A Thermally Reversible Dynamic Bond as a Magnetic and Nonlinear Optical Switch

Xue-Li Cao,[1,2,3]† Jin Liu,[1,2,3]† Chuan-Qi Shen,[1,2] Shu-Qi Wu,[4]* Zi-Shuo Yao,[5] Qing Li,[1,2,3] Zhong-Min Cao,[1,2,3] Lu-Yao Liu,[1,2,3] Fu-Lin Lin,[1,2] Zi-Ang Nan,[1,2] Zhu Zhuo,[1,2] Wei Wang,[1,2] Osamu Sato,[4] and You-Gui Huang[1,2,3]*

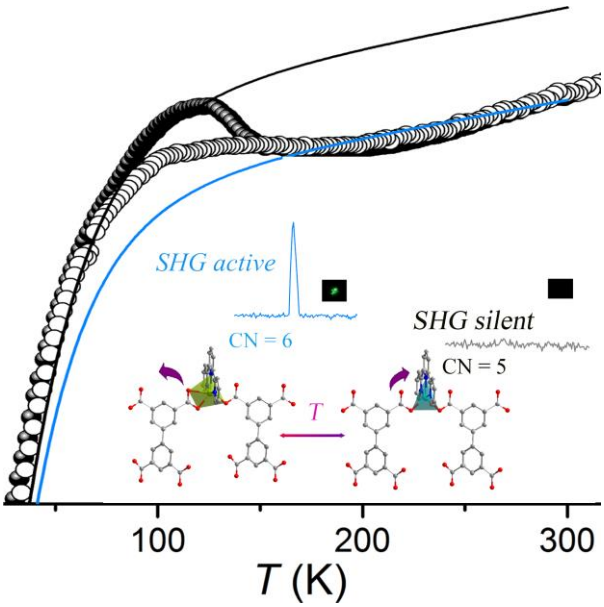

A dynamic coordination bond in a flexible MOF drives the MOF to undergo a thermo-induced reversible phase transition. During the transition, the metal ion Co^{II} exhibits a coordination-mode switching between five- and six-fold and the framework switches between a distorted polar framework and a regular nonpolar framework. Thus, the dynamic bond enables a subtle change of the magnetic property and a substantial change of the nonlinear optical property of the MOF.